Impact of oxygen related extended defects on silicon diode characteristics

J. Vanhellemont,[a] E. Simoen, A. Kaniava,[b] M. Libezny, and C. Claeys

IMEC, Kapeldreef 75, B-3001 Leuven, Belgium

The electrical activity of extended lattice defects formed by interstitial oxygen precipitation in silicon is studied. Their impact on diode characteristics and on minority carrier lifetime is addressed for different initial oxygen contents and pretreatments. The carrier traps present in the substrate are studied with deep level transient spectroscopy and with photoluminescence spectroscopy. The obtained electrical results are correlated with those of structural and chemical characterization using cross-section transmission electron microscopy and Fourier transform infrared spectroscopy. © *1995 American Institute of Physics.*

10.1063/1.359209

I. INTRODUCTION

Precipitation outside the active device area of the excess interstitial oxygen which is inevitably present in Czochralski-grown (Cz) silicon, can have a beneficial influence on device characteristics due to the gettering effect of the oxygen related extended lattice defects. At the same time however, oxygen precipitation has some undesired impact not only on mechanical properties by a lowering of the mechanical strength but also on the electrical properties of silicon substrates by, e.g., the formation of thermal donors or a decrease of the minority-carrier lifetime by the creation of recombination centers. A recent review on the behavior and properties of oxygen in silicon can be found, e.g., in Ref. 1. It has been also known for more than a decade that oxygen precipitation related defects can lead to increased diode leakage currents[2-4] and to increased metal-oxide-semiconductor leakage.[5] Recently the electrical activity of these defects is receiving a renewed interest due to the increased use of internal gettering schemes in advanced processing technologies.[6-9]

Despite this long research effort, the problem of the electrical activity of oxygen precipitation related extended defects in silicon is far from being sorted out. At the present day, it is not even unambiguously determined whether it is the silicon oxide precipitate—and mainly its interface with the surrounding silicon—or the dislocations and stacking faults which often accompany growing SiO_x precipitates, which are the cause of the electrical activity. Much of the older results were also obtained on silicon material which was not processed under the cleanest conditions, leading to an inevitable introduction of metal contamination and, thus, an uncontrolled decoration of the dislocation cores and precipitate interfaces.

In the present article, results are presented in a combined effort to elucidate this problem by the cross correlation of observations obtained with complementary characterization techniques in order to address the impact of oxygen precipitation on the electrical properties of silicon substrates and on diode characteristics.

II. EXPERIMENT

n^+p diodes are fabricated on Czochralski-grown wafers with different starting interstitial oxygen contents and on epi-wafers (Table I). Three wafers from each oxygen content are selected and processed together. Before the diode processing different thermal pretreatments are performed: the first wafer from each set receives no pretreatment (no), the second has a silicon oxide precipitate nucleation step at 750 °C for 8 h (nucl) and the third one has a full internal gettering (IG) treatment. This IG sequence consists of an oxygen out diffusion step at 1100 °C for 6 h, followed by the same nucleation step as the second wafer. The precipitation step is the field oxidation step of the diode process which consists of a 10 h treatment at 975 °C. To serve as an "oxygen-free" reference, a p-type floating zone (FZ) wafer is also included in the diode process. A set of n-type Cz silicon substrates with similar oxygen contents received the same heat treatments and is also listed in Table I. No diodes, however were fabricated on these substrates. In the present study two types of diodes were used, i.e., perimeter diodes consisting of a meander with an area of 10 times 900 μm×30 μm and square area diodes of 900 μm × 900 μm.

After the diode process, the current-voltage (I-V) and capacitance-voltage (C-V) characteristics of the diodes are measured. The I-V characteristics of the diodes are measured using an HP 4145 parameter analyzer. The potential of the back-side substrate contact is varied, while the front-side diode contact is kept grounded. The system leakage is less than 1 pA. The current is measured through the smaller front contact. Attention has also been given to an accurate determination of the doping density by means of C-V analyses, using a 100 kHz, 30 mV ac modulation signal.

Capacitance deep-level transient spectroscopy (DLTS), based on the lock-in principle, is used to determine the position in the band gap and the density and depth profile of the deep levels present within the depletion region of the diodes. Measurements are performed on the p-type substrates over a temperature range from 77 to 450 K to investigate the presence and characteristics of carrier traps within the depleted area of the diodes.

After removal of the diode structures by etching and mechanical polishing, the minority carrier lifetime in all substrates is determined by using the light-induced infrared ab-

---

[a]Electronic mail: vanhellemont@imec.be
[b]On leave from Vilnius University, Sauletekio Avenue 10, 2054 Vilnius, Lithuania.

TABLE I. Experimental matrix used in the present work: wafers with different starting interstitial oxygen content (O_i before) and pretreatments. The interstitial oxygen content after the full diode process is also listed (O_i after) as well as the extended defect density and defect lean zone estimated from the HVEM analyses. The effective carrier lifetime determined with the light induced (LIA) and microwave (MWA) absorption techniques are also given. (— =not measured; * for the epiwafers τ_{eff} corresponds with the lifetime in the substrate).

Sample	O_i before (10^{17} cm^{-3})	O_i after (10^{17} cm^{-3})	Pretreatment	Defects (10^9 cm^{-3})	Defect lean zone (μm)	Effective carrier lifetime (μs) LIA	Effective carrier lifetime (μs) MWA
			p-type Cz				
T6	8.0	8.0	no	<1	-	9.8	6.9
T7	7.4	-	nucl	<1	-	12	5.8
T8	7.3	-	IG	<1	-	11	6.0
T1	9.3	9.0	no	1-2	-	8.3	4.2
T2	9.2	-	nucl	1-2	-	3.8	1.6
T3	9.2	8.7	IG	1	-	7.4	3.2
T26	11.1	3.0	no	50	3	0.46	0.62
T28	10.8	3.1	IG	10	10	0.68	0.75
			p-type epi				
T31	-	-	no	-	-	0.11*	-
T32	-	-	nucl	-	-	0.10*	-
T33	-	-	IG	-	-	0.11*	-
			p-type FZ				
W7	-	-	IG	-	-	14	-
			n-type Cz				
T21	7.3	7.3	no	<1	-	15	17
T22	7.3	-	nucl	<1	-	15	24
T23	7.2	7.2	IG	<1	-	17	20
T16	9.6	-	no	-	-	0.79	1.0
T17	9.5	-	nucl	-	-	0.99	1.2
T11	10.2	6.7	no	10	6	0.72	1.0
T12	10.0	6.8	nucl	10	2	0.92	1.2
T13	9.9	5.8	IG	3	30	1.1	1.1

sorption (LIA) technique[10] which yields information on the lifetime under high carrier injection conditions ($\approx 5 \times 10^{17}$ carriers cm^{-3}) and by using 10 GHz microwave absorption (MWA) measurements to determine the lifetime under moderate injection conditions ($\approx 5 \times 10^{15}$ carriers cm^{-3}). About 50 μm of silicon is polished away from both sides of the samples so that the lifetime in the bulk of the wafer is addressed. The final sample thickness varies between 550 and 570 μm. For both techniques the beam with 1.06 μm wavelength of a pulsed Nd:YAG laser is used to create excess carriers. The effective carrier lifetime is determined by a least squares fit of the asymptotic part of the excess carrier decay. Averages of 50 transients per curve are recorded using a digital oscilloscope with 8 bit conversion and 20 MHz sampling.

Photoluminescence spectroscopy (PL) analyses are performed on polished samples to analyze also the defect related radiative recombination centers in the substrate. A Bio-Rad Fourier transform set up is used to record the PL spectra at 4 K.

The interstitial oxygen concentration before and after the diode process (Table I) is determined from the maximum absorption coefficient at room temperature of the 1106 cm^{-1} band, using the IOC-88 calibration factor of 3.14×10^{17} cm^{-3}/cm^{-1}.[11] The Fourier transform infrared (FTIR) measurements are performed with a Bruker IFS 66v instrument equipped with a cooled MCT-detector.

Specimens for cross-sectional transmission electron microscopy (TEM) are prepared in the conventional way of grinding, polishing, dimpling, and Ar-ion milling. High-voltage TEM is used to characterize the bulk defects and to estimate the defect density and distribution. The TEM analyses are performed on the Jeol 1250 microscope of the University of Antwerp (UCA) with an electron acceleration voltage of 1000 kV.

III. OBSERVATIONS AND DISCUSSION

A. Diode characteristics

The C-V measurements show that the boron concentration in the *p*-type wafers is in the range of $6-10 \times 10^{14}$ cm^{-3} (Table II). No significant influence of the oxygen content and pretreatments on the carrier concentration is observed.

Vanhellemont *et al.*

TABLE II. Ideality factor m, bulk leakage current density J_R, perimeter leakage density J_P, surface generation velocity s_0, forward current intercept J_{f0}, diffusion component J_{d0}, and calculated recombination lifetime τ_r taking into account perimeter effects and diode ideality. (* calculated for a 10^{18} cm^{-3} substrate doping).

Wafer	N_D (10^{14} cm^{-3})	m	J_R (nA cm^{-2})	J_P (pA cm^{-1})	s_0 (cm s^{-1})	J_{f0} (pA cm^{-2})	J_{d0} (pA cm^{-2})	τ_r (μs)
Epi wafers								
T31 no	8.9	1.037	<0.1	3.0	2.5	4.3	2.6	0.075*
T32 nucl	8.9	1.036	<0.1	3.4	-	3.6	2.5	0.078*
T33 IG	8.9	1.032	<0.1	4.0	-	2.7	1.7	0.17*
Low O_i								
T6 no	6.8	1.095	<0.1	3.1	-	88	52	32
T7 nucl	6.3	1.090	<0.1	2.5	-	100	63	25
T8 IG	6.3	1.078	<0.1	3.2	-	73	50	40
Medium O_i								
T1 no	9.9	1.181	0.2	3.3	2.8	330	160	1.6
T2 nucl	9.7	1.194	0.2	4.4	-	540	250	0.66
T3 IG	10.0	1.121	0.1	2.9	2.6	160	74	7.2
High O_i								
T26 no	9.1	1.204	9.6	37.8	2.0	1700	880	0.062
T28 IG	9.4	1.142	0.4	4.1	2.3	470	250	0.75

The area or bulk leakage current component is separated from the perimeter component by combining the leakage current (at a fixed reverse bias) of an area diode with a large area (A_1) to perimeter (P_1) ratio with the leakage current of a perimeter diode with a much smaller area (A_2) to perimeter (P_2) ratio. The area (J_A) and perimeter (J_P) leakage current densities can then be solved from the linear set of equations

$$I_{R1} = J_A A_1 + J_P P_1$$
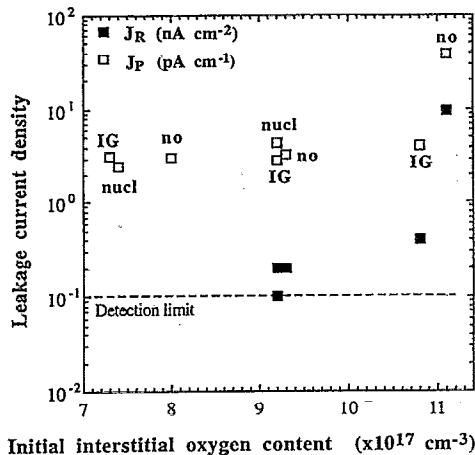$$I_{R2} = J_A A_2 + J_P P_2. \tag{1}$$

FIG. 1. J_R and J_P for the p-type substrates as a function of the initial interstitial oxygen content and thermal pretreatment.

Figure 1 shows the volume generation leakage current density J_R and the perimeter generation leakage current density J_P as a function of the initial interstitial oxygen content. The perimeter component consists of two contributions: one which is related with the interface between the oxide and the silicon substrate and which depends on the interface trap density and one which is related with the bulk traps present in the near surface perimeter depletion region of the diode. Measurements performed on gated diodes on the same wafers showed that the first component depends little or not on the oxygen content in the substrate and that in all cases the variation of the second, substrate dependent component, is largely dominating the change of perimeter leakage. Average values are given obtained on 10 diodes. The spread on the measured currents is of the order of 20%. For the low and medium oxygen content wafers there is little influence of the oxygen and of the pretreatment. In the high oxygen content wafers one clearly sees an increase of both perimeter and bulk leakage current. The internally gettered wafer on the other hand behaves similar as the lower oxygen content wafers.

From the I-V characteristics information can be obtained on the generation and recombination lifetimes. Using Shockley–Read–Hall (SRH) theory one can write the total forward current I_F as the sum of bulk and space-charge-region recombination components, I_r and I_d, respectively.

$$I_F = I_r + I_d \tag{2}$$

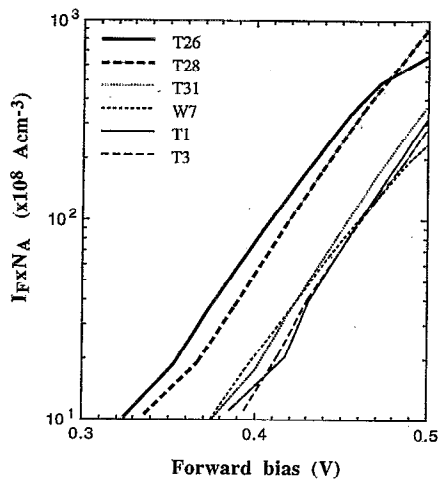with for a forward bias larger than 0.25 V

FIG. 2. Typical $I_F \times N_A$ vs V characteristics for the diodes used in the present study. A strong impact of the initial oxygen content is only observed for the wafers with the highest O_i.

FIG. 3. Inverse τ_g and τ_r for the p-type substrates as a function of the initial interstitial oxygen content and thermal pretreatment.

$$I_r \approx I_{0r} e^{qV/2kT}$$

and

$$I_d \approx I_{0d} e^{qV/kT}. \tag{3}$$

The generation lifetime τ_g can in principle be calculated from the generation current density J_g which can be obtained from the reverse current density J_R (obtained after subtraction of the perimeter component). The recombination lifetime τ_r can be calculated from the reverse current extrapolated to zero bias which gives an estimate of the diffusion component of the leakage current.[8]

As shown in Table II and also in Fig. 1, even for the large 900 μm $\times$900 μm diodes used in the present study, the reverse current is in many cases too small to be measured accurately so that the generation and recombination lifetime cannot always be calculated from the reverse characteristics. For this purpose gated diodes with a two times larger area were used which were fabricated on the same wafer.

The recombination lifetime τ_r can however also be calculated from the forward current density of the conventional diodes extrapolated to zero bias (J_{F0}). For a strongly asymmetrical n^+p junction as used in the present study, one can assume that emitter and emitter-contact recombination is negligible with respect to recombination in the lower doped substrate.[8] J_{F0} is then given by

$$J_{F0} = J_{d0} + J_{r0}$$

with

$$J_{d0} \approx q \sqrt{\frac{D_n}{\tau_r}} \frac{n_i^2}{N_A}. \tag{4}$$

D_n is the electron (minority carrier) diffusion coefficient and N_A is the dopant concentration. A more accurate recombination lifetime can be obtained by correcting for perimeter effects and for diode ideality as discussed elsewhere.[12]

Equation (4) suggests that to compare the forward characteristics of diodes fabricated on substrates with different resistivity one has to take into account the dopant concentra-
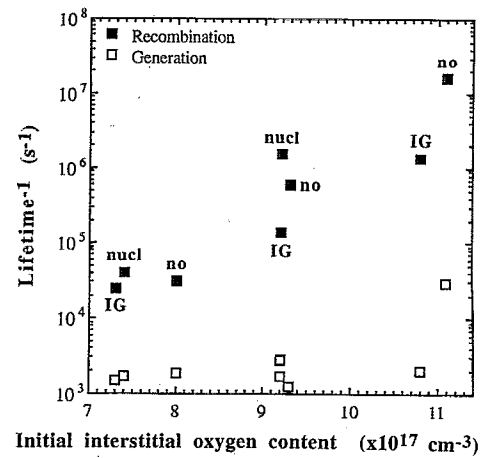
tion. Figure 2 shows typical $I_F \times N_A/V$ curves for the substrates used in the present study. For the substrates with the highest oxygen content there is a dramatic increase of the forward current (and intercept J_{F0}).

Figure 3 shows the inverse (=proportional to the trap density) generation and recombination lifetimes, τ_g and τ_r, respectively, calculated from the diode characteristics. Here again the IG wafer with high oxygen content behaves like the lower oxygen content wafers while the high oxygen content wafer without denuding step shows a much shorter lifetime. A similar behavior is observed for the ideality factor m of the diodes.

In the presence of trapping centers the generation and recombination lifetime are connected by the relationship[13]

$$\tau_g \approx \tau_r \exp\left(\frac{|E_T - E_i|}{kT} \right). \tag{5}$$

E_T is the energy level of the trapping center while E_i is the intrinsic level.

For samples T26 (high oxygen, no), T28 (high oxygen, IG), T1 (medium oxygen, no) and T2 (medium oxygen, nucl), where the leakage current is clearly increased by the presence of generation/recombination centers, the ratio τ_g/τ_r is about 500 leading to a trap level of $E_T \approx E_i \pm 0.16$ eV, i.e., $E_c - 0.4$ eV or $E_v + 0.4$ eV at room temperature.

B. TEM analyses

Figure 4 shows a cross-section high-voltage electron microscopic image of the near surface area of samples T26 and T28 which have the highest initial oxygen content and also the highest precipitation related defect density. The figure illustrates the defect lean zone (DLZ) of about 3 and 10 μm near the surface for the wafer without pretreatment and with an internal gettering treatment, respectively. Deeper in the bulk the typical defects are observed: precipitate/dislocation complexes (PD), isolated plate-like SiO_x precipitates (P). The higher magnification images of typical bulk defects in Fig. 4, show also a small bulk stacking fault (SF) with a central silicon oxide precipitate of which a low density is also observed in the internal gettered high oxygen content

Vanhellemont *et al.*

FIG. 4. Top: HVEM micrograph illustrating the bulk defect distribution in T26 (3 μm DLZ) and T28 (10 μm DLZ). Bottom: Higher magnification of typical extended lattice defects related with interstitial oxygen precipitation: stacking faults (SF), silicon oxide precipitates (P) and precipitate/dislocation complexes (PD).
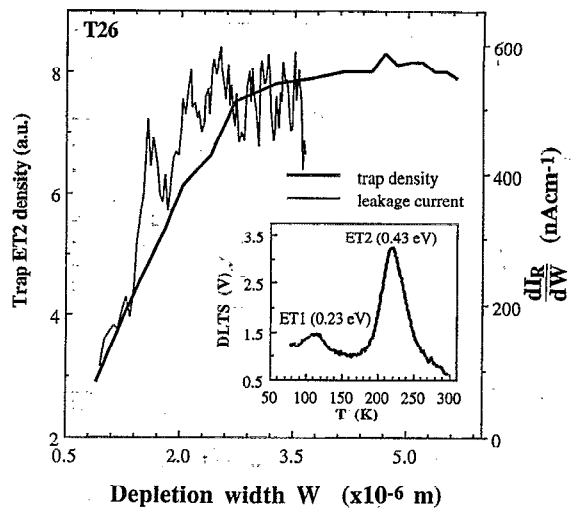

FIG. 5. Depth profile of the density of minority carrier trap ET2 and of the derivative of the leakage current (dI_R/dW) with respect to the depletion width for a high oxygen content wafer with 5×10^{10} cm^{-3} oxygen related precipitate/dislocation complexes (PD's) in the substrate. The PD lean zone of about 3 μm near the wafer surface is clearly reflected in the depth profiles.

wafers. In all cases the density of PD's is at least one order of magnitude higher than that of isolated precipitates and at least two orders of magnitude higher than the SF density. As illustrated in Table I, for the p-type substrates, the TEM analyses reveal that the precipitate density in the bulk of the wafers depends strongly on the starting interstitial oxygen content and on the thermal pretreatment. For the highest oxygen content wafers, the bulk precipitate density in the wafer without pretreatment is about 5 times higher than in the IG wafer.

The TEM analyses also show that the average PD and precipitate size is larger in T28 (IG) than in T26 (no). This is related with the much larger critical precipitate radius which corresponds with the first high temperature out-diffusion step. Only the largest precipitate nuclei (with a low density) survive the high temperature of the out-diffusion step and will grow to a larger size. In the high oxygen content n-type wafers the amount of precipitated oxygen is only half of that in the corresponding p-type substrates which is reflected also in the observed lower defect density which is about 1×10^{10} cm^{-3} for T11 and T12 and only 3×10^9 cm^{-3} for T13.

From Fig. 4 it can be concluded that the IG treatment results in the formation of a defect lean zone (DLZ) of about 10 μm in the high oxygen content wafers. The wafer without pretreatment has a DLZ of about 3 μm. The DLTS depth profile shown in Fig. 5 is recorded on the same substrate and corresponds thus well with the extended defect distribution observed with TEM. This suggests a close correlation between the observed minority traps and the oxygen related extended defects. A recent study[14] of similar extended defects using temperature dependent electron beam induced current imaging revealed in n-type substrates dislocation related deep levels at estimated positions of 0.1 and 0.4 eV from the conduction band edge in good agreement with the present DLTS and TEM results.

Taking into account the substrate dopant concentration of about 10^{15} cm^{-3} for the wafers listed in Table II, the depleted zone of the diode varies between 1 and 10 μm for a reverse bias between 0 and 20 V. Only in the T26 wafer (high initial oxygen content, no pretreatment), the depleted area can thus reach deep enough to "see" extended defects.

C. DLTS results

In the I-V measurements an increase of one order of magnitude of the leakage current is observed when the edge of the depleted area reaches the edge of the denuded zone which is of the order of 3 μm for sample T26. The derivative of the leakage current with respect to the depletion width (dI_R/dW), gives an idea of the variation of the carrier lifetime and thus also of the deep level density with depth below the junction. Increasing the depletion width well above 2 μm, leads to the observation of two minority (electron) traps ET1 and ET2 in the DLTS spectra as shown in the inset in Fig. 5. Both the DLTS and I-V measurements yield a similar depth profile suggesting that the leakage current is most likely generated by deep level ET2. For lower reverse bias or
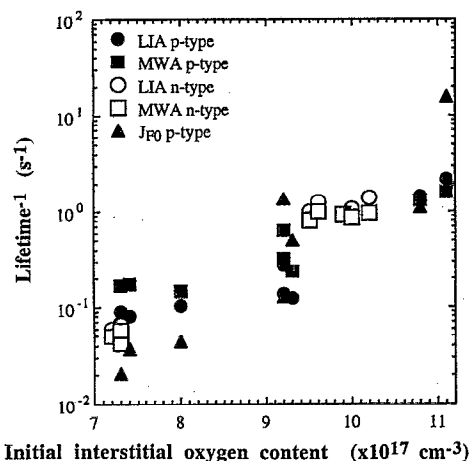
FIG. 6. Inverse recombination carrier lifetime measured from electrical and optical/microwave measurements as a function of the initial oxygen content and pretreatment. An exponential dependence of the carrier recombination center density on the initial oxygen content is observed.

low oxygen content samples, no deep levels are observed, in good agreement with the excellent leakage current values which are of the order of 0.1 nA cm^{-2} at 6 V reverse bias. No hole (majority) traps are observed in the present study in contrast with previous studies using Schottky barriers[15–17] where broad bands associated with majority traps were observed. ET2, the minority trap closest to midgap has a position in the bandgap of $E_c - 0.43$ eV close to the value estimated from the generation/recombination lifetime ratio and an estimated capture cross-section σ_n at 240 K of 10^{-14} cm^2. Chan et al.[4] reported an electron (minority) trap with the same trap parameters and density in n^+p gated diodes formed in high oxygen content substrates after a low/high-temperature treatment. As nucleation step they used a 800 °C treatment for 16 h while the precipitation step was a 16 h treatment at 1050 °C. The minority carrier recombination lifetime which they calculated from the diode characteristics is of the order of 0.2–0.3 μs, in good agreement with the value obtained for T26 (high O$_i$, no) and T28 (high O$_i$, IG). An electron (majority) trap with the same position in the band gap was recently also reported in n-type Cz silicon.[18]

D. Lifetime measurements

The results of the effective lifetime measurements are summarized in Table I while the minority carrier recombination lifetime calculated from the forward diode characteristics is listed in Table II. For the epiwafers the doping of the substrate (10^{18} cm^{-3}) was used for the calculation. The (inverse) recombination lifetime results are also summarized in Fig. 6 as a function of the initial interstitial oxygen content. An exponential decrease of the effective lifetime with increasing initial oxygen content is observed. The minority carrier lifetime in the low oxygen content substrates is comparable to that in the FZ silicon substrate. The agreement between the lifetimes listed in Tables I and II is remarkably good taking into account that the lifetimes are calculated for strongly different injection conditions and that furthermore, both LIA and MWA are measuring the bulk lifetime averaged

over the whole wafer thickness while the diode characteristics are mainly obtained in the near surface region of the wafer where the oxygen related extended defect density in most devices is lower than in the bulk.

As the wafers are relatively thin and the surfaces were not passivated, the effective carrier lifetime determined from the asymptotic part of the carrier decays is strongly affected by surface recombination and one can write

$$\frac{1}{\tau_{\text{eff}}} = \frac{1}{\tau_s} + \frac{1}{\tau_b}, \qquad (6)$$

with τ_s and τ_b the surface and bulk recombination lifetime, respectively. Without surface passivation, the surface recombination lifetime is of the order of 10 μs. For that reason only for the samples with much smaller τ_{eff}, the surface recombination is negligible and the effective lifetime can be assumed to be equal to the bulk carrier lifetime. The bulk lifetime depends on the level of carrier injection (Δn) and is given by[15]

$$\frac{1}{\tau_b} = A + B\Delta n + C\Delta n^2 = \frac{1}{\tau_{\text{SRH}}} + \frac{1}{\tau_{\text{rad}}} + \frac{1}{\tau_{\text{Auger}}}. \qquad (7)$$

For low injection levels (MWA) both the radiative (τ_{rad}) and Auger (τ_{Auger}) components can be neglected.

The SRH lifetime is, in general, injection level dependent and becomes $\tau_{\text{SRH}}(11) = \tau_r$ for low level (11) injection. τ_r is the microscopic lifetime of minority carriers. This carrier lifetime is inversely proportional to the concentration of recombination centers N_t and their capture cross section σ_n, with

$$\tau_{\text{SRH}} \approx \frac{1}{\sigma_n v_{th} N_t}. \qquad (8)$$

v_{th} ($\approx 10^7$ cm s^{-1}) is the thermal velocity of the carriers.

Assuming for T26 that $\tau_r \approx 0.75$ μs and that the trap at $E_c - 0.43$ eV with an estimated trap density of 10^{12} cm^{-3} is responsible for this lifetime, one can calculate an effective capture cross section at room temperature of about 10^{-13} cm^2 in reasonable agreement with the value of 10^{-14} cm^2 at 240 K obtained from a standard Arrhenius analysis of the DLTS results.

Chan et al.[4] used a power law relation to fit τ_g values with the trap density N_t:

$$N_t = A\tau_g^{-n}. \qquad (9)$$

Assuming $n = 1$ and with $N_t \approx 10^{12}$ cm^{-3} and $\tau_g \approx 33$ μs (for T26) and 480 μs (for T28), one obtains $A \approx 3.3 \times 10^7$ and 4.8×10^8 s cm^{-3}, respectively, in good agreement with the values of Chan et al.[4] which range from 2 to 4.5×10^8 s cm^{-3}.

E. PL results

As illustrated in Fig. 7, PL analyses reveal in the samples with medium and high oxygen content, as most prominent features, the well known D1 and D2 lines at 807 and 874 meV, respectively.[19] The origin of the D bands in silicon is believed to be either linked with impurity-related optical transitions near the dislocation core or to be an intrinsic
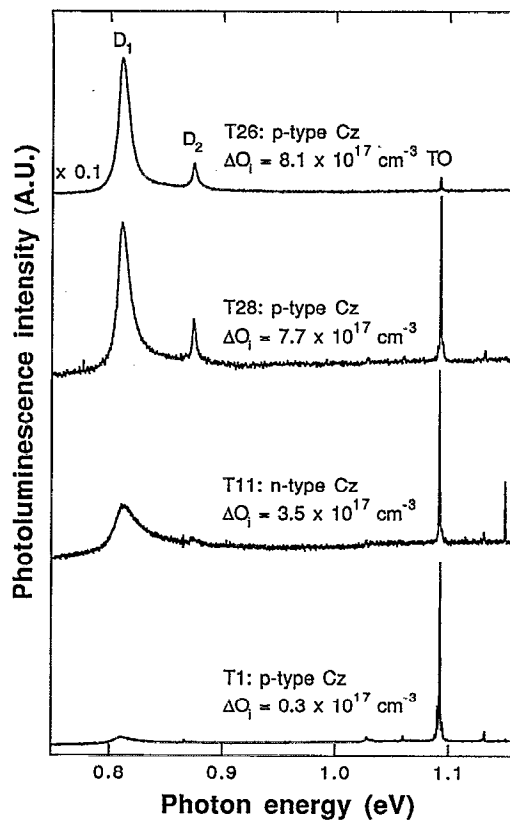
Vanhellemont et al.

FIG. 7. PL spectra as a function of the precipitated amount of oxygen for the p- and n-type wafers (Ref. 21).

property of the dislocation. In the last case, the position of the PL lines might be correlated with the edge component of the Burgers vector of the dislocations.[20]

Figure 8 illustrates that there exists a linear correlation between the normalized PL amplitude of the D1 line and the inverse of the carrier lifetime for carrier lifetimes larger than 1 μs. As a more or less constant ratio is observed between the amplitudes of the D1 and D2 lines, the same behavior is observed for D2. This suggests that the recombination at 4 K and at room temperature occurs through the same recombination centers which are connected with the dislocation
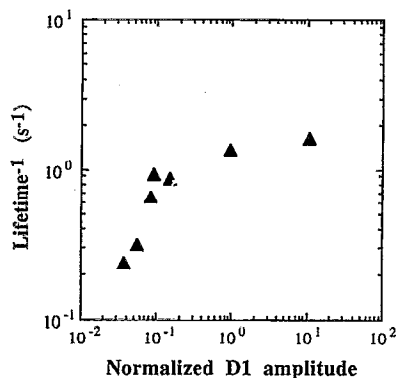

FIG. 8. Correlation between the normalized amplitude of the D1 line and the inverse minority carrier lifetime measured by MWA.

loops surrounding the silicon oxide precipitates. More PL results and their correlation with low-temperature FTIR measurements have been published elsewhere.[21]

If one follows the suggestion of Lelikov et al.[20] that the position of the PL lines is correlated with the edge component (=strain) of the Burgers vector of dislocations one can write in first order approximation:

$$E_{PL} = E_g - A \left(\frac{b_e}{a} \right)^2. \qquad (10)$$

b_e is the edge component of the Burgers vector, a the lattice constant of silicon, and A (≈ 0.8 eV) a constant which is related with the deformation potential and the effective carrier mass. Under this assumption D1 would correspond with 90° dislocation [$(b_e/e)^2 = \frac{1}{2}$] segments which are the dislocation types present in the prismatic punching systems surrounding silicon oxide precipitates. The dominant D2 line would then correspond with 60° dislocation segments as Eq. (10) yields for $(b_e/a)^2 = \frac{3}{8}$ an energy level of 870 meV in agreement with the position of D2.

The PL results in correlation with the DLTS and TEM observations thus suggest that D1 and D2 are connected with the dislocation complexes surrounding the silicon oxide precipitates and that they might be associated with two electron traps of 0.23 and 0.43 eV below the conduction band.

IV. CONCLUSIONS

The results of the present study show that the observed impact of oxygen precipitation related lattice defects on carrier lifetime in p-type substrates is mainly related to their activity as trap for minority carriers. A close correlation is observed between the PD density and distribution, the leakage current increase and the carrier lifetime decrease.

PL analyses reveal a close correlation between the D1 and D2 line intensities and the minority carrier lifetime indicating that the same recombination centers are active. The D1 and D2 lines might correspond with the minority carrier traps E_c-0.43 eV and E_c-0.23 eV, respectively, observed with DLTS. The TEM observations suggest that D1 and D2 are correlated with 60° and 90° dislocations.

By making the proper corrections for perimeter effects and diode ideality, a quantitative correlation between minority carrier trap characteristics derived from DLTS and the observed minority carrier lifetimes and leakage currents is possible using standard SRH theory.

[1] H. Bender and J. Vanhellemont, "Oxygen in Silicon," in Handbook on Semiconductors, edited by T. S. Moss and S. Mahajan (Elsevier, New York, 1994), Vol. 3, pp. 1637–1753.
[2] S. N. Chakravarti, P. L. Garbarino, and K. Murty, Appl. Phys. Lett. 40, 581 (1982).

[3] J. W. Slotboom, M. J. Theunissen, and A. J. R. de Kock, IEEE Trans. Electron Devices **EDL-4**, 403 (1983).

[4] S. S. Chan, C. J. Varker, J. D. Whitfield, and R. W. Carpenter, Mater. Res. Soc. Symp. Proc. **46**, 281 (1985).

[5] K. D. Beyer, S. Chakravarti, P. L. Garbarino, and K. Yang, J. Electrochem. Soc. **134**, 1753 (1987).

[6] K. Katayama, A. Agarwal, Z. J. Radzimski, and F. Shimura, Jpn. J. Appl. Phys. **32**, 298 (1993).

[7] Y. Murakami, Y. Satou, H. Furuya, H. Abe, and T. Shingyouji, Electrochem. Soc. Extended Abstracts **93-2**, 422 (1993).

[8] Y. Murakami and T. Shingyouji, J. Appl. Phys. **75**, 3548 (1994).

[9] J. Vanhellemont, E. Simoen, G. Bosman, C. Claeys, A. Kaniava, E. Gaubas, A. Blondeel, and P. Clauws, Electrochem. Soc. Proc. **94-10**, 670 (1994).

[10] J. Vaitkus, E. Gaubas, K. Jarasiunas, and M. Petrauskas, Semicond. Sci. Technol. A **7**, 131 (1992).

[11] A. Baghdadi, W. Bullis, M. Croarkin, Y-Z. Li, R. Scace, R. Series, P. Stallhofer, and M. Watanabe, J. Electrochem. Soc. **136**, 2015 (1989).

[12] J. Vanhellemont, E. Simoen, and C. Claeys, Appl. Phys. Lett. **66** (1995).

[13] D. K. Schroder, J. M. Hwang, J. S. Kang, A. M. Goodman, and B. L. Sopori, Electrochem. Soc. Proc. **85-5**, 419 (1985).

[14] T. Sekiguchi, S. Kusanagi, B. Shen, and K. Sumino, Electrochem. Soc. Proc. **94-10**, 659 (1994).

[15] D. K. Schroder, *Semiconductor Materials and Device Characterization* (Wiley, New York, 1990).

[16] J. M. Hwang and D. K. Schroder, J. Appl. Phys. **59**, 2476 (1986).

[17] K. Schmalz, F.-G. Kirscht, H. Klose, H. Richter, and K. Tittelbach-Helmreich, Phys. Status Solidi A **100**, 567 (1987).

[18] H. S. Kim, E. K. Kim, and S. K. Min, J. Appl. Phys. **69**, 6979 (1991).

[19] K. Weronek, J. Weber, and H. J. Queisser, Phys. Status Solidi A **137**, 543 (1993).

[20] Y. Lelikov, Y. Rabane, S. Ruvimov, D. Tarhin, A. Sitnikova, and Y. Shreter, Mater. Sci. For. **83–87**, 1321 (1992).

[21] J. Vanhellemont, P. Clauws, M. Libezny, E. Simoen, and C. Claeys, Proceedings of the 22nd International Conference on the Physics of Semiconductors, Vancouver, Canada, August 14–19, 1994 (to be published).

5676   J. Appl. Phys., Vol. 77, No. 11, 1 June 1995

Vanhellemont *et al.*